Nanoscale

RSC Publishing

PAPER

View Article Online
View Journal

Development of gadolinium based nanoparticles having an affinity towards melanin†

Cite this: DOI: 10.1039/c2nr33457g

Jessica Morlieras,[a] Jean-Michel Chezal,[bcd] Elisabeth Miot-Noirault,[bcd] Amandine Roux,[ef] Laurence Heinrich-Balard,[ef] Richard Cohen,[efg] Sébastien Tarrit,[bcd] Charles Truillet,[a] Anna Mignot,[ahi] Roxanne Hachani,[a] David Kryza,[ag] Rodolphe Antoine,[j] Philippe Dugourd,[j] Pascal Perriat,[h] Marc Janier,[ag] Lucie Sancey,[a] François Lux*[a] and Olivier Tillement[a]

Received 2nd November 2012
Accepted 10th December 2012

DOI: 10.1039/c2nr33457g

www.rsc.org/nanoscale

Small Rigid Platforms (SRPs) are sub-5 nanometre gadolinium based nanoparticles that have been developed for multimodal imaging and theranostic applications. They are composed of a polysiloxane network surrounded by gadolinium chelates. A covalent coupling with quinoxaline derivatives has been performed. Such derivatives have proven their affinity for melanin frequently expressed in primary melanoma cases. Three different quinoxaline derivatives have been synthesised and coupled to the nanoparticles. The affinity of the grafted nanoparticles for melanin has then been shown *in vitro* by surface plasmon resonance on a homemade melanin grafted gold chip.

Published on 12 December 2012 on http://pubs.rsc.org | doi:10.1039/C2NR33457G
Downloaded by University of California - San Diego on 21 January 2013

Introduction

Human melanoma, characterized by an uncontrolled development of melanocytes producing the melanin pigment, is a widespread aggressive skin cancer. Once inaccessible to surgery, it is mainly resistant to treatment by chemo- and radiotherapy.[1–4] Since median survival time for patients with metastatic melanoma with stage III or IV is limited (about 6–16 months),[5–7] there is an urgent need to develop agents succeeding in an earlier and more effective diagnosis and being able to treat disseminated melanoma.[1,8–10]

Our group has been synthesizing ultrasmall multifunctional gadolinium-based nanoparticles associating imaging and therapeutic activities. These nanoparticles were validated for multimodal imaging (MRI, SPECT, CT, fluorescence imaging) and for radiotherapy thanks to their radiosensitizing properties.[11–13] The last generation of nanoparticles is called Small Rigid Platforms (SRPs) and it displays about ten DOTA (1,4,7,10-tetraazacyclododecane-1,4,7,10-tetraacetic acid) derivatives grafted on a polysiloxane network. Due to the synthesis process of the nanoparticles, some of the DOTA ligands are chelating Gd^{3+} ions while the other DOTA molecules remain free. These free DOTA ligands are available to chelate other cations of interest (*e.g.* ^{111}In for SPECT imaging) and/or to perform amide bonds with NH_2-ended molecules *via* one of the carboxylic acid arms.[11] SRPs are attractive in terms of size (3–5 nm), enabling efficient renal clearance[14] with an appropriate circulation time in the bloodstream. These SRPs are likely to take advantage of tumour vasculature abnormalities, *e.g.* porous vessels,[15] to reach tumour tissue by the Enhanced Permeability and Retention (EPR) effect.[16] This passive targeting might be reinforced by an active one to establish tumour-selective diagnosis and to be promising for targeted-therapy.[17] The covalent conjugation of an effective melanoma vector to the surface of the SRPs might enhance tumour uptake and will be first tested *in vitro*.

Melanin is an amorphous and random copolymer of brown-black eumelanin and yellow to reddish brown pheomelanin, both derived from the common precursor dopaquinone.[18] Dopaquinone which is formed by the oxidation of tyrosine by tyrosinase is a highly reactive intermediate.[19] Its intramolecular cyclization gives rise to the formation of eumelanin while the presence of thiols in glutathione or cysteine leads to

[a]*Laboratoire de Physico-Chimie des Matériaux Luminescents, UMR 5620 CNRS – Université Claude Bernard Lyon 1, Université de Lyon, 69622 Villeurbanne Cedex, France. E-mail: francois.lux@univ-lyon1.fr; Tel: +33 472431200*

[b]*Inserm UMR 990 – BP 184, Clermont-Ferrand, 63005 Cedex, France*

[c]*Clermont Université, UMR 990 – Université d'Auvergne, BP 10448, 63000 Clermont-Ferrand, France*

[d]*Centre Jean Perrin, 63011 Clermont-Ferrand, France*

[e]*Université Claude Bernard Lyon 1, Université de Lyon, 69622 Villeurbanne Cedex, France*

[f]*Matériaux, Ingénierie et Sciences, INSA Lyon, UMR 5510 CNRS – Université de Lyon, ISPB-Faculté de Pharmacie, F-69373 Lyon, France*

[g]*Hôpitaux de Lyon, Hôpital Edouard Herriot, Laboratoire de Biochimie et Biologie moléculaire et Service de médecine nucléaire, 69437 Lyon Cedex 03, France*

[h]*Matériaux, Ingénierie et Sciences, INSA Lyon, UMR 5510 CNRS – Université de Lyon, 69621 Villeurbanne Cedex, France*

[i]*Nano-H SAS, 38070 Saint-Quentin Fallavier, France*

[j]*Laboratoire de Spectrométrie Ionique et Moléculaire, UMR 5579 CNRS – Université Claude Bernard Lyon 1, 69622 Villeurbanne Cedex, France*

† Electronic supplementary information (ESI) available. See DOI: 10.1039/c2nr33457g

Published on 12 December 2012 on http://pubs.rsc.org | doi:10.1039/C2NR33457G
Downloaded by University of California - San Diego on 21 January 2013

cysteinyldopas, underlying the formation of pheomelanin by oxidation of the thiol adducts.[20,21]

Melanin pigment, detected in more than 90% of primary melanoma cases[22] and found in 40–50% of all metastatic lesions,[23] could be a promising target for melanoma-targeting strategy of SRPs. Indeed, metastatic melanomas are fast growing tumors showing numerous areas of necrosis and containing extracellular melanin released from death cells. Extracellular melanin, only present in the melanoma environment, is therefore attractive for specific tumor-targeting concept as demonstrated by Dadachova *et al.*[24,25] for radioimmunotherapy of melanoma. Nevertheless the radiolabeled anti-melanin mAb (^{99m}Tc-6D2) used in this study displayed a noticeable and long lasting kidney uptake after i.v. injection in nude mice. Furthermore, 6D2 mAb is only produced in very small quantities. In this context, several tumour-specific tracers have been investigated over the last decades, including a series of benzamide (BZA) derivatives.[26–30] The replacement of the benzene moiety contained in BZAs by a heteroaromatic structure, particularly coplanar fused rings, proved a high affinity of such molecules toward pigmented melanoma.[31] This affinity may be due in part to the π stacking interaction between the polycyclic aromatic block of the targeting agent and the aromatic ones of the melanin subunits.[9,32] An ionic interaction occurring between the tertiary amine of the melanin-targeting ligand being protonated and the negative charges borne by melanin might also ease the binding to melanin. In this context, a quinoxaline derivative (ICF01012) which has already shown high, specific and long-lasting binding to melanin in animal models has been selected as a melanoma-seeking agent to be grafted to SRPs.[9,33,34] However the targeting properties of the quinoxaline derivatives might be highly altered by their coupling to the SRPs. We have opted to introduce into the ICF01012 scaffold an aliphatic primary amino group, which can be easily modified and facilitate the grafting to SRPs. Keeping in mind the importance of the steric hindrance as well as the ionic and hydrophobic sites on the binding to melanin, two different positions of linkage (*i.e.* aromatic and aliphatic parts) have been designed. For the aromatic approach, we have chosen to replace the iodine atom with an amino pegylated-urea residue (melanin-targeting ligand **3** – Scheme 3). As for the aliphatic strategy, amino function has been introduced into the N-terminal ethyl residue directly, or through a pegylated spacer (melanin-targeting ligands **1** and **2** – Scheme 1 and 2 respectively).

Owing to the melanin heterogeneous structure[35] and to the difficulties of performing optical spectroscopy on such a macromolecule,[36–38] surface plasmon resonance appeared to be a very adapted technology to highlight the binding of functionalized SRPs to melanin. The literature described surface plasmon resonance biosensor as an interesting technique to detect and characterize biomolecular interactions in real time.[39] BIAcore® is a conventional surface plasmon resonance system where a thin gold film is coated to a prism, which reflects the incident light.[40] The gold surface is covered with a carboxymethylated dextran matrix, which enables the covalent conjugation of any receptor biomolecule. Surface plasmon resonance arises through the interaction of the evanescent wave created by total internal reflection with delocalized surface electrons in the gold film at the interface with the medium of lower refractive index (solution). This interaction excites collective resonant oscillation named plasmon. The field strength is amplified as a result of plasmon resonance. Surface plasmon resonance is used to probe the refractive index of the aqueous layer immediately adjacent to the gold surface. Surface plasmon resonance is seen as a drop in the intensity of the reflected light. To study an interaction, one partner (the ligand) is immobilized onto the surface and the other (the analyte) is flowed past the surface of the sensor chip through a microfluidic flow cell.[41] When the two partners interact to form a complex, the refractive index is changed near the gold surface which modifies the angle of incidence required to create the surface plasmon resonance phenomenon. This change in the refractive index which is closely correlated with the change in mass near the gold surface is measured in real-time and the signal obtained is plotted in resonance unit (RU) *versus* time to give a sensorgram.[42,43]

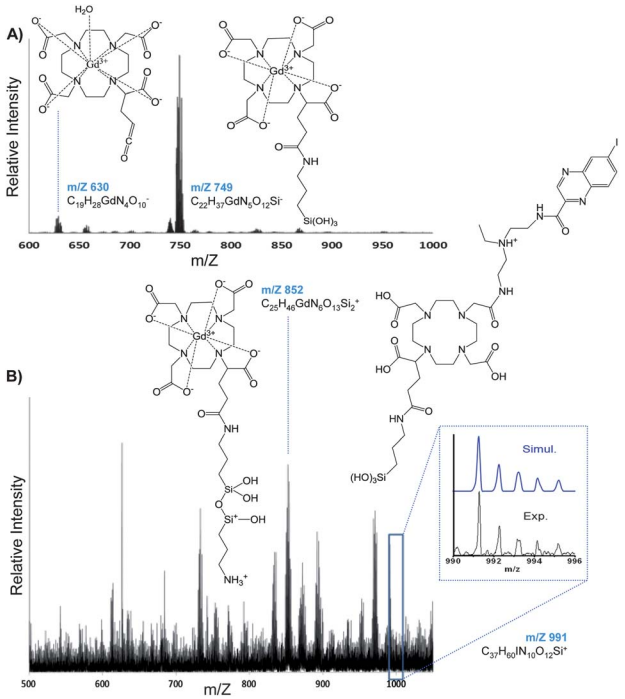

Fig. 1 (A) Low *m*/*z* part of the ESI mass spectrum recorded for SRP-**1** in a negative mode. (B) Low *m*/*z* part of the ESI mass spectrum recorded for SRP-**1** in a positive mode.

In this work, we describe the syntheses of the three melanin-targeting ligands as well as their covalent conjugation to SRPs. Afterwards and in order to select the best candidate for melanoma-targeting, the binding of synthesized SRPs to melanin has been assessed by surface plasmon resonance assays.

Materials and methods

Chemicals

Synthesis of the melanin-targeting ligands. All reagents and solvents were purchased from the following commercial suppliers: Sigma-Aldrich, Acros organics, Carlo Erba. Column chromatography was performed with Merck neutral aluminium oxide 90 standardized (63–200 μm) or SDS silica gel 60AC.C35-

Downloaded by University of California - San Diego on 21 January 2013
Published on 12 December 2012 on http://pubs.rsc.org | doi:10.1039/C2NR33457G

70 μm, chromagel. Thin layer chromatography (TLC) was performed on Merck neutral aluminium oxide $60F_{254}$ plates or Merck silica gel $60F_{254}$ plates. The plates were visualized with UV light (254 nm) and/or by development with iodine, ninhydrin (0.2% in ethanol) or potassium permanganate (0.5% in 2.5% aqueous sodium carbonate solution). Melting points were determined on an electrothermal IA9300 (capillary) and were not corrected. NMR spectra 200 MHz for ^{1}H or 50 MHz for ^{13}C were recorded on a Bruker Avance 200 instrument (Bruker Biospin, Wissembourg, France) using $CDCl_3$, CD_3OD or DMSO-d_6 as solvents. Chemical shifts were referenced by theresidual solvent signals relative to tetramethylsilane at 0 ppm. Infrared spectra were recorded in KBr pellets or CCl_4 on a FT vector 22 or on an IRTF Nicolet IS10 instrument with attenuated total reflectance (ATR) accessory (ν expressed in cm^{-1}). Electrospray ionization mass spectra (ESI-MS) were obtained on a TSQ 7000 ThermoQuest Finnigam (Les Ulis, France). The samples were analyzed in CH_3OH/H_2O (1/1, v/v, containing 1% HCOOH) or CH_3CN/H_2O (1/1, v/v, containing 1% HCOOH) in positive mode or in CH_3OH/H_2O (1/1, v/v, containing 1% NH_4OH) in negative mode, at a final concentration of 8–12 pmol μL^{-1}. Each ESI-MS spectrum was recorded by averaging 10 spectra. Microanalyses were performed by Analytical Laboratory of the CNRS (Vernaison, France) for the elements indicated and were within 0.4% of the theoretical values unless indicated. All air-sensitive reactions were run under argon atmosphere. All solvents were dried using common techniques.[44]

SRP functionalization with melanin-targeting ligands. *N*-(3-Dimethylaminopropyl)-*N*′-ethylcarbodiimide hydrochloride (EDC, >98.0%), *N*-hydroxysuccinimide (NHS, >97.0%), gadolinium chloride hexahydrate ([$GdCl_3 \cdot 6H_2O$], 99%), sodium hydroxide (NaOH, 99.99%), hydrochloric acid (HCl, 36.5–38%), sodium chloride (NaCl, >99.5%), dimethyl sulfoxide (DMSO, >99.5%), acetonitrile (CH_3CN, >99.9%) and trifluoroacetic acid (TFA, >99%) were purchased from Aldrich® Chemical (France) and used without further purification. The SRPs synthesis has been already described elsewhere.[11] The core–shell nanoparticles (core: gadolinium oxide and shell: polysiloxane) and the SRPs were purchased from Nano-H SAS (Saint-Quentin Fallavier, France) and the DOTAGA anhydride (1,4,7,10-tetraazacyclododecane-1-glutaric anhydride-4-7-10-triacetic acid) was purchased from CheMatech (Dijon, France). For the preparation of an aqueous solution of nanoparticles, only milli-Q water (ρ >18 MΩ cm) was used.

Surface plasmon resonance assays. HBS-P (HEPES buffer) was purchased from GE Healthcare® and used as running buffer. For immobilization, amine coupling reagents were obtained from the GE Healthcare® kit containing 0.2 M EDC in water and 0.05 M NHS in water and ethanolamine–HCl pH 8.5. The melanin ligand was purchased from Aldrich® and beforehand dissolved at 20 mg mL^{-1} in a 1 N ammonium hydroxide (NH_4OH) solution.[45]

Experimental

Synthesis of melanin-targeting ligand 1 (Scheme 1)

Step 1. Synthesis of N-*[2-[*N-*ethyl*-N-*(2-bocaminoethyl)amino] ethyl]phthalimide (**S2**).* To a solution of 2-(boc-amino)ethyl bromide[46] (909 mg, 3.57 mmol) in anhydrous acetonitrile (15 mL) were added under argon, potassium carbonate (984 mg, 7.14 mmol) and *N*-[2-(ethylamino)ethyl]phthalimide hydrochloride salt[47] (**S1**) (500 mg, 1.35 mmol). The reaction mixture was stirred at 60 °C (external temperature) for 48 h and the solvent was evaporated under reduced pressure. The residue was taken up with a saturated aqueous sodium carbonate solution (20 mL) and extracted with dichloromethane (4 × 20 mL). The organic layers collected were dried over magnesium sulfate, filtered and evaporated under reduced pressure. The residue obtained was purified by alumina column chromatography using a dichloromethane/ethanol solution (99/1, v/v) as eluent to give **S2** (544 mg, 1.51 mmol) as a yellow oil. Yield 42%. R_f Al_2O_3/CH_2Cl_2/EtOH (99/1, v/v) 0.32; IR (ATR diamond accessory) ν 3317, 2975, 2619, 1708, 1655, 1517, 1471, 1392, 1169 cm^{-1}; ^{1}H NMR ($CDCl_3$) δ 0.93 (t, 3H, J = 7 Hz), 1.38 (s, 9H), 2.55 (m, 4H), 2.70 (t, 2H, J = 6.4 Hz), 3.12 (q, 2H, J = 5.5 Hz), 3.74 (t, 2H, J = 6.4 Hz), 5.03 (brs, 1H), 7.70 (m, 2H), 7.83 (m, 2H); ^{13}C NMR ($CDCl_3$) δ 11.7, 28.4 (3C), 36.4, 38.2, 47.3, 51.3, 52.7, 78.8, 123.3 (2C), 132.1 (2C), 134.0 (2C), 156.1, 168.5 (2C); ESI-SM *m*/*z* 362.21 $[M + H]^+$.

Step 2. Synthesis of tert-*butyl* N-*[2-[*N-*(2-aminoethyl)*-N-*ethyl-amino]ethyl]carbamate (**S3**).* To a stirred solution of **S2** (480 mg, 1.33 mmol) in ethanol (25 mL) was added hydrazine monohydrate (646 μL, 13.3 mmol). The mixture was stirred at room temperature for 18 h. After cooling to 0 °C, the white precipitate was filtered and washed with ethanol (2 × 5 mL). The filtrate was evaporated under reduced pressure and the residue was purified by alumina chromatography using dichloromethane/ethanol solution (8/2, v/v) as eluent to give **S3** (241 mg, 1.04 mmol) as a yellow oil. Yield 78%. R_f Al_2O_3/CH_2Cl_2/EtOH (8/2, v/v) 0.22; IR (ATR diamond accessory) ν 3400–3100, 2973, 1668, 1531, 1474, 1167 cm^{-1}; ^{1}H NMR ($CDCl_3$) δ 0.93 (t, 3H, J = 7 Hz), 1.37 (s, 9H), 1.54 (se, 2H), 2.45 (m, 6H), 2.66 (t, 2H, J = 5.8 Hz), 3.09 (q, 2H, J = 5.8 Hz), 5.09 (se, 1H); ^{13}C NMR ($CDCl_3$) δ 11.6, 28.4 (3C), 38.5, 39.7, 47.6, 52.9, 56.4, 78.9, 156.1; ESI-SM *m*/*z* 232.07 $[M + H]^+$.

Step 3. Synthesis of N-*[2-[*N-*ethyl*-N-*(2-bocaminoethyl)amino] ethyl]-6-iodoquinoxaline-2-carboxamide (**S4**).* To a solution of **S3** (230 mg, 0.99 mmol) in anhydrous tetrahydrofuran (15 mL) was added under argon *p*-nitrophenyl 6-iodoquinoxaline-2-carboxylate[48] (419 mg, 0.99 mmol). The mixture was stirred at room temperature for 17 h before addition of dichloromethane (30 mL). The resulting solution was poured into a 1 N aqueous sodium hydroxide solution (90 mL) and extracted with dichloromethane (3 × 40 mL). The organic layers were combined, washed with a 5% aqueous sodium carbonate solution (2 × 50 mL), dried over magnesium sulfate, filtered and evaporated under reduced pressure. The residue obtained was purified by alumina column chromatography using a dichloromethane/ethanol solution (99/1, v/v) as eluent to give **S4** (447 mg, 0.87 mmol) as a white solid. Yield 88%; mp 77–79 °C; R_f Al_2O_3/CH_2Cl_2/EtOH (99/1, v/v) 0.22; IR (CCl_4) ν 2975, 1718, 1685, 1521, 1170 cm^{-1}; ^{1}H NMR ($CDCl_3$) δ 1.06 (t, 3H, J = 7.1 Hz), 1.34 (s, 9H), 2.64 (m, 4H), 2.73 (t, 2H, J = 6 Hz), 3.20 (q, 2H, J = 5.8 Hz), 3.56 (q, 2H, J = 6 Hz), 5.22 (se, 1H), 7.85 (d, 1H, J = 8.8 Hz), 8.04 (dd, 1H, J = 1.8, 8.8 Hz), 8.31 (m, 1H), 8.58 (d, 1H,

Published on 12 December 2012 on http://pubs.rsc.org | doi:10.1039/C2NR33457G
Downloaded by University of California - San Diego on 21 January 2013

$J = 1.8$ Hz), 9.63 (s, 1H); ^{13}C NMR ($CDCl_3$) δ 11.9, 28.4 (3C), 37.2, 38.8, 47.6, 52.8, 53.0, 79.2, 98.1, 130.9, 138.6, 139.5, 139.7, 144.0, 144.5, 144.7, 156.0, 162.9; ESI-SM m/z 514.17 $[M + H]^+$.

Step 4. Synthesis of N-*[2-[*N*-ethyl*-N-*(2-aminoethyl)amino]ethyl]-6-iodoquinoxaline-2-carboxamide trihydrochloride salt (*i.e. *melanin-targeting ligand **1**).* To a solution of **S4** (200 mg, 0.39 mmol) in anhydrous dichloromethane (15 mL) was added under argon an anhydrous ethereal solution of 2 N hydrochloric acid (4 mL). The reaction mixture was stirred at room temperature for 13 h and the solvent was evaporated under reduced pressure. The residue was taken up with an anhydrous diethyl ether (5 mL), filtered and dried overnight in a desiccator to afford compound **1** (172 mg, 0.33 mmol) as a white solid. Yield 85%. mp 127–129 °C; IR (KBr) ν 3317, 2977, 2641, 1668, 1532, 1474 cm^{-1}; ^{1}H NMR (DMSO-d_6) δ 1.27 (t, 3H, $J = 7.1$ Hz), 3.38 (m, 8H), 3.78 (m, 2H), 3.56 (q, 2H, $J = 6$ Hz), 7.92 (d, 1H, $J = 8.8$ Hz), 8.64 (dd, 1H, $J = 1.8$, 8.8 Hz), 8.32 (m, 3H), 8.64 (d, 1H, $J = 1.8$ Hz), 9.38 (m, 1H), 9.45 (s, 1H), 10.88 (s, 1H); ^{13}C NMR (DMSO-d_6) δ 8.4, 33.4, 33.8, 47.8, 48.6, 50.6, 99.7, 130.8, 137.6, 139.0, 139.9, 143.6, 144.3, 144.5, 163.6; ESI-SM m/z 414.19 $[M + H]^+$; elemental analysis calcd for $C_{15}H_{20}IN_5O$, 3HCl, H_2O: C: 33.32; H: 4.66; N: 12.95; Cl: 19.67. Found: C: 33.21; H: 4.29; N: 12.78; Cl: 17.42%.

Synthesis of melanin-targeting ligand 2 (Scheme 2)

Step 1. Synthesis of N-*[2-[2-(2-*tert*-butoxycarbonylaminoethoxy) ethoxy]ethyl]acrylamide (**S6**).* Compound **S6** was obtained by reacting *tert*-butyl 2-[2-aminoethoxy]ethoxy]ethyl carbamate[47] (**S5**) and acryloyl chloride in the presence of diisopropylethylamine as described by Alterman *et al.*[49] Yield 83%. IR (KBr) 3459, 3400–3300, 1718, 1678, 1506, 1367, 1174, 1144, 1108 cm^{-1}; ^{1}H NMR ($CDCl_3$) δ 1.42 (s, 9H), 3.30 (m, 3H), 3.50 (m, 10H), 5.64 (dd, 1H, $J = 4$, 8 Hz), 6.22 (d, 1H, $J = 4$ Hz), 6.23 (d, 1H, $J = 8$ Hz).

Step 2. Synthesis of tert*-butyl [2-[2-[3-[*N*-ethyl*-N-*[2-[(6-iodoquinoxaline-2-carbonylamino)ethyl]amino] propionylamino]ethoxy] ethoxy]ethylcarbamate (**S8**).* To a solution of *N*-[2-(*N*-ethylamino) ethyl]-6-iodoquinoxaline-2-carboxamide (**S7**)[48] (400 mg, 1.08 mmol) in anhydrous acetonitrile (20 mL) were added under argon, silica gel (800 mg) and a solution of the acrylamide derivative **S6** (489 mg, 1.62 mmol) in anhydrous acetonitrile (10 mL). The reaction mixture was stirred at reflux for 72 h and the solvent was evaporated under reduced pressure. The residue was purified by alumina column chromatography using a chloroform/ethanol solution (99/1, v/v) as eluent to afford compound **S8** (172 mg, 0.33 mmol) as a light brown oil. Yield 66%. R_f Al_2O_3/$CHCl_3$/EtOH (99/1, v/v) 0.16; IR (ATR diamond accessory) ν 3400–3250, 2971, 2932, 2870, 1667, 1530, 1165 cm^{-1}; ^{1}H NMR ($CDCl_3$) δ 1.05 (t, 3H, $J = 7$ Hz), 1.38 (s, 9H), 2.35 (t, 2H, $J = 6$ Hz), 2.65 (q, 2H, $J = 7$ Hz), 2.75 (m, 4H), 3.33. (m, 4H), 3.50 (m, 10H), 5.11 (se, 1H), 7.78 (d, 1H, $J = 8.8$ Hz), 7.85 (m, 1H), 8.03 (dd, 1H, $J = 1.5$, 8.8 Hz), 8.29 (m, 1H), 8.56 (d, 1H, $J = 1.5$ Hz), 9.59 (s, 1H); ^{13}C NMR ($CDCl_3$) δ 11.6, 28.4 (3C), 33.5, 37.7, 38.9, 40.3, 47.4, 49.7, 52.1, 70.0 (4C), 79.5, 98.1, 130.7, 138.6, 139.5, 139.8, 144.0, 144.4, 144.6, 156.0, 163.2, 172.4; ESI-SM m/z 673.43 $[M + H]^+$.

Step 3. Synthesis of N-*[2-[*N*-ethyl*-N-*[2-[2-(2-aminoethyl)ethoxy] ethylcarbamoyl]amino]ethyl]-6-iodoquinoxaline-2-carboxamide (*i.e. *melanin-targeting ligand **2**).* A solution of **S8** (303 mg, 0.45 mmol) in trifluoroacetic acid (5 mL) was stirred under argon at room temperature for 1 h 30 min. The reaction mixture was evaporated under reduced pressure and the residue was taken up with water (10 mL), an aqueous saturated sodium carbonate solution (20 mL) and dichloromethane (10 mL). After decantation, the aqueous layer was extracted with dichloromethane (3 × 25 mL) and the organic layers collected were dried over anhydrous magnesium sulfate, filtered and evaporated to dryness to give compound **2** (252 mg, 0.44 mmol) as a light brown oil which was used without further purification. Yield 98%. IR (KBr) ν 3500–3100, 2923, 2853, 1690–1600, 1534, 1127 cm^{-1}; ^{1}H NMR ($CDCl_3$) δ 1.03 (t, 3H, $J = 7$ Hz), 2.34 (t, 2H, $J = 6$ Hz), 2.59 (q, 2H, $J = 7$ Hz), 2.74 (m, 4H), 3.36 (m, 2H), 3.55 (m, 12H), 7.77 (d, 1H, $J = 8.8$ Hz), 7.93 (m, 1H), 8.01 (dd, 1H, $J = 1.7$, 8.8 Hz), 8.35 (m, 1H), 8.54 (d, 1H, $J = 1.7$ Hz), 9.56 (s, 1H); ^{13}C NMR ($CDCl_3$) δ 11.6, 33.5, 37.7, 38.9, 41.6, 47.4, 49.7, 52.1, 70.1 (4C), 98.1, 130.7, 138.5, 139.4, 139.7, 143.9, 144.3, 144.5, 163.2, 172.4; ESI-SM m/z 573.13 $[M + H]^+$.

Synthesis of melanin-targeting ligand 3 (Scheme 3)

Step 1. Synthesis of N-*(2-diethylaminoethyl)-6-nitroquinoxaline-2-carboxamide (**S10**).* To a stirred solution of *N*,*N*-diethylethylenediamine (2.00 mL, 14.23 mmol) in anhydrous dichloromethane (40 mL) was added at 0 °C, under argon, a 2 M trimethylaluminium solution in hexane (7.14 mL, 14.28 mmol). After 10 min, a solution of ethyl 6-nitroquinoxaline-2-carboxylate (**S9**)[9] (2.35 g, 9.51 mmol) in anhydrous dichloromethane (30 mL) was added and the mixture was refluxed for 3 h. After cooling to room temperature, water (60 mL) was added. After decantation, the aqueous layer was extracted with dichloromethane (3 × 40 mL). The organic layers were combined, dried over magnesium sulfate, filtered and evaporated under reduced pressure. The residue obtained was purified by alumina column chromatography using a solution of dichloromethane/ethanol (97/3, v/v) as eluent to give compound **S10** (2.71 g, 8.54 mmol) as a yellow solid. Yield 90%. R_f Al_2O_3/dichloromethane/ethanol (97/3, v/v) 0.71; mp 83–85 °C; IR (KBr) ν 3384, 2967, 2931, 2811, 1685, 1529, 1342 cm^{-1}; ^{1}H NMR ($CDCl_3$) δ 1.08 (t, 6H, $J = 7$ Hz), 2.61 (q, 4H, $J = 7$ Hz), 2.71 (t, 2H, $J = 6$ Hz), 3.57 (q, 2H, $J = 7$ Hz), 8.27 (d, 1H, $J = 9$ Hz), 8.44 (m, 1H), 8.28 (dd, 1H, $J = 2.5$, 9.2 Hz), 9.05 (d, 1H, $J = 2.5$ Hz), 9.80 (s, 1H); ^{13}C NMR ($CDCl_3$) δ 12.2 (2C), 37.5, 47.2 (2C), 51.4, 124.1, 125.8, 131.5, 142.8, 146.2 (2C), 148.8, 162.2, C–NO_2 carbon not found. ESI-SM m/z 318.06 $[M + H]^+$.

*Step 2. Synthesis of 6-amino-*N*-(2-diethylaminoethyl)quinoxaline-2-carboxamide (**S11**).* A stirred solution of **S10** (3.30 g, 10.4 mmol) in ethanol (330 mL) was hydrogenated (1 atm) at room temperature over 10% Pd/C (330 mg) for 4 h. The black suspension was filtered through celite 545, washed with ethanol (20 mL) and the filtrate was concentrated under reduced pressure. The residue obtained was purified by alumina column chromatography using a solution of dichloromethane/ethanol (97/3, v/v) as eluent to give compound **S11** (2.34 g, 8.14 mmol) as a yellow solid. Yield 78%. R_f Al_2O_3/dichloromethane/ethanol (97/3, v/v) 0.27; mp 171–173 °C; IR (KBr) ν 3397, 3214, 2969, 2802, 1655, 1613, 1491, 1297, 1221 cm^{-1}; ^{1}H NMR ($CDCl_3$) δ 1.06 (t, 6H, $J = 7$ Hz), 2.60 (q, 4H, $J = 7$ Hz), 2.69 (t, 2H, $J = 6$ Hz), 3.54

Published on 12 December 2012 on http://pubs.rsc.org | doi:10.1039/C2NR33457G
Downloaded by University of California - San Diego on 21 January 2013

(q, 2H, $J = 7$ Hz), 4.52 (se, 2H), 7.19 (m, 2H), 7.82 (d, 1H, $J = 8.9$ Hz), 8.27 (m, 1H), 9.44 (s, 1H); ^{13}C NMR ($CDCl_3$) δ 12.1 (2C), 37.4, 47.2 (2C), 51.8, 107.5, 122.8, 131.0, 135.2, 140.1, 144.1, 145.9, 149.6, 164.0; ESI-SM m/z 288.09 $[M + H]^+$.

*Step 3. Synthesis of 6-[3-[2-[2-(2-*tert*-butyloxycarbonyl aminoethoxy)ethoxy]ethyl]ureido]-*N*-(2-diethylaminoethyl)quinoxaline-2-carboxamide (**S12**).* To a stirred solution of **S11** (500 mg, 1.74 mmol) in anhydrous dichloromethane (50 mL) were added under argon, anhydrous pyridine (418 mL, 5.17 mmol) and *p*-nitrophenyl chloroformate (386 mg, 1.19 mmol). The reaction mixture was stirred at room temperature for 30 min and evaporated under reduced pressure. The crude product was taken up with anhydrous diethyl ether (40 mL) and filtered to give the unstable *p*-nitrophenyl carbamate hydrochloride salt (830 mg, 1.7 mmol) as an orange solid. The latter was dissolved under argon in anhydrous tetrahydrofuran (40 mL) before addition of anhydrous triethylamine (237 mL, 5.17 mmol) and *tert*-butyl 2-[2-aminoethoxy]ethoxy]ethyl carbamate[19] (**S5**). The solution was stirred at room temperature for 24 h and evaporated under reduced pressure. The crude product was dissolved in dichloromethane (60 mL) and washed with a 1 N aqueous sodium hydroxide solution (4 × 45 mL). The organic layer was dried over magnesium sulfate, filtered and evaporated to dryness. The residue was purified by alumina column chromatography using a solution of dichloromethane/ethanol (97/3, v/v) as eluent to give compound **S12** (762 mg, 1.36 mmol) as a gum. Yield 80%. R_f Al_2O_3/dichloromethane/ethanol (97/3, v/v) 0.19; IR (ATR diamond accessory) ν 3400–3100, 2971, 2932, 2872, 1668, 1525, 1491, 1213 1132 cm^{-1}; ^{1}H NMR (CD_3OD) δ 1.12 (t, 6H, $J = 7$ Hz), 1.42 (s, 9H), 2.69 (q, 4H, $J = 7$ Hz), 2.77 (m, 2H), 3.23 (t, 2H, $J = 5.6$ Hz), 3.48 (m, 16H), 7.90 (dd, 1H, $J = 2.4$, 9.1 Hz), 8.30 (d, 1H, $J = 2.4$ Hz), 9.37 (s, 1H); ^{13}C NMR (CD_3OD) δ 10.4 (2C), 27.4 (3C), 36.5, 39.4, 39.9, 46.8 (2C), 51.2, 69.7, 69.8, 69.9 (2C), 80.1, 114.0, 125.7, 131.3, 138.0, 143.0, 144.5, 144.9, 145.8, 157.3, 158.4, 165.6; ESI-SM m/z 562.43 $[M + H]^+$.

*Step 4. Synthesis of 6-[3-[2-[2-(2-aminoethoxy)ethoxy]ethyl]ureido]-*N*-(2-diethylaminoethyl)quinoxaline-2-carboxamide (*i.e. *melanin-targeting ligand **3**).* Compound **3** was prepared according to the procedure developed for the last step of synthesis of **2** starting from 6-[3-[2-[2-(2-*tert*-butyloxycarbonylaminoethoxy) ethoxy]ethyl]ureido]-*N*-(2-diethylaminoethyl)quinoxaline-2-carboxamide (**S12**) (667 mg, 1.19 mmol). The residue was purified by alumina column chromatography using a solution of dichloromethane/ethanol/ammonium hydroxide (90/10/1, v/v/v) as eluent to give compound **3** (508 mg, 1.10 mmol) as a yellow solid. Yield 93%. mp 100–102 °C; R_f Al_2O_3/dichloromethane/ethanol/ammonium hydroxide (90/10/1, v/v/v) 0.36; IR (KBr) ν 3400–3050, 3000–2750, 1684, 1635, 1521, 1489, 1351, 1212, 1134 cm^{-1}; ^{1}H NMR ($CDCl_3$) δ 1.08 (t, 6H, $J = 7$ Hz), 2.15 (se, 2H), 2.52 (q, 4H, $J = 7$ Hz), 2.72 (t, 2H, $J = 6.2$ Hz), 3.05 (t, 2H, $J = 5.6$ Hz), 3.60 (m, 12H), 6.15 (m, 1H), 7.82 (d, 1H, $J = 2.4$ Hz),7.97 (d, 1H, $J = 9.3$ Hz), 8.30 (m, 1H), 8.38 (dd, 1H, $J = 2.4$, 9.3 Hz), 9.53 (s, 1H), 9.80 (se, 1H); ^{13}C NMR ($CDCl_3$) δ 12.1 (2C), 37.4, 39.8, 41.2, 47.1 (2C), 51.6, 69.7, 69.9 (2C), 71.6, 113.2, 124.4, 130.1, 136.5, 141.4, 143.7, 143.9, 144.8, 155.7, 163.7; ESI-SM m/z 462.23 $[M + H]^+$.

Covalent conjugation of the melanin-targeting ligands to SRPs. Syntheses were performed at room temperature. SRP concentrations are stated in mol L^{-1} of gadolinium(III) element. 100 μmol of freeze-dried SRPs were dispersed in water (100 mM) for 15 min and treated by EDC and NHS at pH 5 for 30 min (EDC/NHS/Gd molar ratio 2.4 : 2.4 : 1). The activated SRP solution was divided into four aliquots: three to be grafted with each of the three NH_2-ended melanin-targeted ligands (respectively **1**, **2** and **3**) and a last one to be used as a reference. Each targeting ligand was mixed with one of the previously activated SRP aliquots at pH 7–7.4 for 8 h (targeting ligand/Gd molar ratios: 1.3 : 1 for SRP-**1**, 3.5 : 1 for SRP-**2** and 2.1 : 1 for SRP-**3**). Similarly, the last sample considered as the reference was subjected to the same conditions, *i.e.* previously remaining activated SRP aliquot was stirred at pH 7–7.4 for 8 h. To achieve higher proton longitudinal relaxivities, additional Gd^{3+} ions were inserted to the four SRP aliquots by adding a 100 mM Gd^{3+} solution prepared with $GdCl_3 \cdot 6H_2O$ in water (additional Gd^{3+}/initial Gd molar ratio 0.5 : 1). The final mixture was stirred for 3 h at pH 5–6. Each SRP aliquot was subjected to tangential filtration to a 3000 factor over a 5 kDa membrane to remove any unconjugated product or free Gd^{3+} ions and was freeze-dried for storage, using a Christ Alpha 1-2 lyophilizer. The functionalized freeze-dried SRPs are stable for months without alteration.

Techniques of particle characterization

Relaxivity measurements. Relaxivity experiments were performed on a Bruker® mq60 NMR Analyzer at 37 °C. Samples were measured at a specific Gd(III) concentration, calculated from ICP-OES. Measurements were plotted as $1/T_1$ *vs.* Gd(III) concentration (mM). The slope of this line provides the molar relaxivity.

Inductively Coupled Plasma-Optical Emission Spectroscopy (ICP-OES) analysis. The determination of the accurate concentration of gadolinium in SRP samples was performed by ICP-OES with a Varian® 710-ES spectrometer. First, SRPs were predispersed in water (100 mM). Small amounts of SRP aqueous solutions were diluted and heated at 80 °C for 3 h in 5 mL of concentrated nitric acid (67% HNO_3 (w/w)). Subsequently, the samples were scattered in 50 mL of water. For the calibration of ICP-OES, single element standard solution was used and prepared from 1000 ppm Gd-standard from SCP Science® by successive dilutions with an HNO_3 5% (w/w) matrix.

Photon Correlation Spectroscopy (PCS) size and ζ-potential measurements. Hydrodynamic diameters (HDs) and ζ-potentials of our samples were determined with a Zetasizer NanoS PCS (Photon Correlation Spectroscopy, laser He–Ne 633 nm) from Malvern Instruments®. For HD measurements, 200 μL of an aqueous solution of SRPs (10 mM) were pipetted into a disposable micro-cuvette (ZEN0040). Attenuator and position were optimized by the device. Prior to ζ-potential experiments, the SRPs (10 mM) were diluted in an aqueous solution containing 0.01 M NaCl and adjusted to the desired pH. ζ-Potential measurements were recorded at 25 °C with palladium electrodes within a high concentration cell (ZEN1010). The ζ-potential was automatically calculated from electrophoretic mobility based on the Smoluchowski equation, $\nu = (\varepsilon E/\eta)\zeta$, where ν is the measured electrophoretic velocity, η is the viscosity, ε is the electrical permittivity of the electrolytic solution and E is the electric field.

Published on 12 December 2012 on http://pubs.rsc.org | doi:10.1039/C2NR33457G
Downloaded by University of California - San Diego on 21 January 2013

Mass spectrometry. Full scan mass experiments were performed using a linear quadrupole ion trap mass spectrometer (LTQ, Thermo Fisher Scientific, San Jose, CA) with enlargement for the high 400–4000 Th range. The nanoparticle solution was electrosprayed at a flow rate of 5 μg min^{-1} in positive ion mode. Isotopic distributions of fragment ions were recorded using the zoom scan mode of the LTQ quadrupole ion trap mass spectrometer.

Infrared spectra. The IR spectra of solid dry SRP samples were acquired on an IRAffinity-1, Shimadzu® with an ATR platform by applying attenuated total reflection Fourier transform infrared (ATR-FTIR) spectroscopy from 600 to 4000 cm^{-1}.

Ultraviolet-visible absorption spectra. Aqueous solutions of SRPs were analyzed by a UV-vis spectrophotometer (Varian Cary50) in the range of 200 to 800 nm, with a Hellma semi-micro cell, 10 mm light path, 1400 μL, manufactured from Suprasil quartz.

Surface plasmon resonance. The surface Plasmon resonance assays were performed using a BIAcore® 2000 biosensor. The instrument was equipped with research-grade CM5 sensorchips (GE Healthcare®, Uppsala, Sweden).

Immobilization of melanin. Immobilization was performed at 32 °C and required two steps. The first step consists in derivatizing the CM5 sensor chip into an amine surface. To this end, ethylenediamine was bound to the carboxymethylated dextran layer of the CM5 sensor chip, using the standard amine coupling kit (GE Healthcare®, Uppsala, Sweden). The flow rate was set at 5 μL min^{-1}. Briefly, the carboxylic acids of the channel 2 (FC2) of the CM5 sensor chip were activated with EDC/NHS for 15 min. Then, ethylenediamine (1 M in a 50 mM borate buffer at pH 8.6) was injected during 15 additional min and the remaining active sites were blocked by adding ethanolamine (1 M at pH 8.5) for 15 min. The second step implies the melanin immobilization. Prior to this immobilization, the carboxylic acids on melanin were activated for 30 min at room temperature by mixing 20 μL of melanin with NH_4OH (1 M),[20] 10 μL of EDC (0.2 M in water) and 20 μL of NHS (0.05 M in water). Then, 150 μL of 10 mM borate buffer was added and the whole mixture was injected in channel 2 at 5 μL min^{-1} for 30 min. As before, remaining active sites were blocked by adding ethanolamine (1 M at pH 8.5) for 5 min. The signal corresponding to immobilized melanin on channel 2 was approximately 200 RU. Channel 1 (FC1) of the CM5 sensor chip was conserved under the carboxymethylated dextran form in order to be used as a reference surface and to observe possible non-specific interactions.

Experiment progress. Binding analyses were performed at 25 °C and the flow rate was set to 20 μL min^{-1}. An experiment gathered data from several cycles. A cycle typically consisted in the injection of the analyte (unfunctionalized and functionalized SRPs with melanin-targeting ligands) for 3 min. This step was followed by a waiting period of 2.5 min under running buffer. Then, the surface was regenerated to remove SRPs from the sensorchip with the injection of 20 mM NaOH and 1 M NaCl for 1.5 min at 20 μL min^{-1}. A waiting period of 2 min under running buffer finished the cycle. Each experiment began with five cycles, called startup, injecting running buffer instead of analyte to stabilize the baseline of the BIAcore®.

Results and discussion

Synthesis of the melanin-targeting ligands

The three melanin-targeting ligands (**1**, **2** and **3**) shown in Fig. 1 were prepared according to the corresponding Schemes 1, 2 and 3. Compound **1** was obtained in four steps starting from *N*-[2-(ethylamino)ethyl]phthalimide hydrochloride salt (**S1**)[47] (Scheme 1). Briefly, alkylation of amine **S1** with *N*-protected aminoethyl bromide[46] gave the tertiary amine **S2**. Selective deprotection of the phthalimide group afforded amine **S3** which was conjugated to *p*-nitrophenyl 6-iodoquinoxaline-2-carboxylate[48] to give amide **S4**. Final *N*-boc deprotection was achieved in an anhydrous ethereal solution of hydrochloric acid to produce ligand **1** as a trihydrochloride salt. Pegylated derivative **2** was obtained by condensation of the previously reported secondary amine **S7**[48] with acrylamide **S6** according to the procedure developed by You, L. *et al.* for aza-michaël addition of amines to α,β-unsaturated amides,[50] followed by acidic removal of the boc group of **S8** (Scheme 2). The synthesis of the aromatic functionalized ligand **3** started from previously reported nitro ester **S9**,[9] a key intermediate in the synthesis of ICF01012 (Scheme 3), was hydrogenated over Pd/C to give the aromatic amine **S11**. In order to introduce the amino pegylated linker we converted the amino function of **S11** into *p*-nitrophenylcarbamate using *p*-nitrophenyl chloroformate. The resulting activated carbamate was isolated as a hydrochloride salt and directly coupled with *tert*-butyl 2-[2-aminoethoxy]ethoxy]ethyl carbamate[19] in the presence of triethylamine to give urea **S12**. Next, the deprotection of *N*-boc group afforded melanin-targeting ligand **3**.

Synthesis – grafting strategy of the melanin-targeting ligands to SRPs

SRPs were synthesised *via* a top-down process according to previous studies.[11] This pathway classically allows SRP synthesis displaying an average 3 nm hydrodynamic diameter (HD) and an average 8.5 kDa molecular mass. SRPs consist in a polysiloxane network around which DOTA derivatives are arranged. The number of DOTA molecules per SRP was estimated to be 10. Around 50% of these DOTA ligands chelate Gd^{3+} ions while others remain free for peptide conjugation.

Thus, SRPs exhibit some available carboxylic acid functions (from free DOTA ligands) for grafting. NH_2-ended melanin-targeting ligands were covalently conjugated to these carboxylic acid functions thanks to an amide bond. The structure of

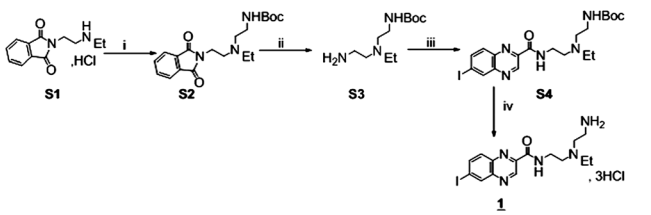

Scheme 1 Synthesis of melanin-targeting ligand **1**. *Reagents and conditions*: (i) 2-(boc-amino)ethyl bromide, potassium carbonate, acetonitrile, 60 °C. (ii) Hydrazine hydrate, ethanol, rt. (iii) *p*-Nitrophenyl 6-iodoquinoxaline-2-carboxylate, tetrahydrofuran, rt. (iv) Dichloromethane, 2 N HCl/diethyl ether, rt.

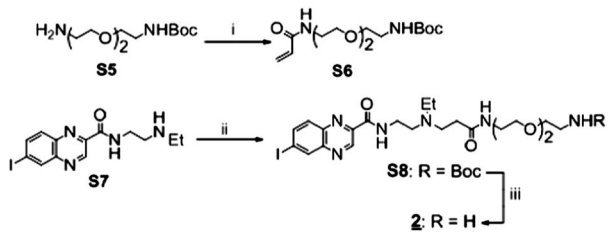

Scheme 2 Synthesis of melanin-targeting ligand **2**. *Reagents and conditions:* (i) acryloyl chloride, *N*,*N*-diisopropylethylamine, rt. (ii) **S6**, SiO_2, acetonitrile, reflux. (iii) Trifluoroacetic acid, rt.

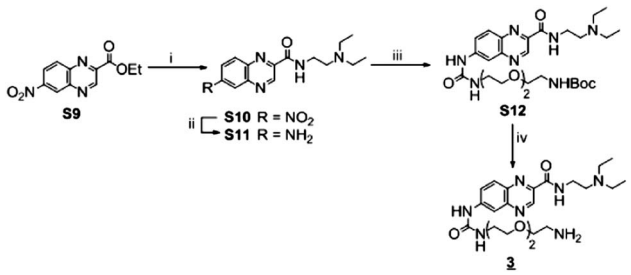

Scheme 3 Synthesis of melanin-targeting ligand **3**. *Reagents and conditions:* (i) *N*,*N*-diethylethylenediamine, trimethylaluminium, 0 °C then reflux. (ii) H_2, Pd/C 10%, EtOH, rt. (iii) (a) *p*-Nitrophenyl chloroformate, pyridine, dichloromethane, rt; (b) **S5**, tetrahydrofuran, rt. (iv) Trifluoroacetic acid, rt.

Published on 12 December 2012 on http://pubs.rsc.org | doi:10.1039/C2NR33457G
Downloaded by University of California - San Diego on 21 January 2013

melanin-targeting ligands **1** and **2** was quite similar, the only difference being the insertion of a pegylated spacer for melanin-targeting ligand **2**. This spacer was added in order to demonstrate the possible influence of a steric hindrance. On the other hand, the two binding sites of melanin-targeting ligand **3** were reversed compared to those of melanin-targeting ligand **2** in order to understand the importance of both ionic and hydrophobic sites.

The HDs of the conjugated SRPs were 4.6 ± 1.3 nm, 3.8 ± 1.0 nm and 4.4 ± 1.3 nm for SRP-**1**, **2** and **3** respectively, showing a significant increase in comparison with the native particles (see ESI†). ζ-Potentials of unfunctionalized and functionalized SRPs with melanin-targeting ligands **1**, **2** and **3** were measured for different pH values. The isoelectric point of the unfunctionalized SRPs was about 4.5, while it slightly increased for the functionalized SRPs with melanin-targeting ligands **1**, **2** and **3** (about 5). This small increase was in good agreement with the surface modification of the SRPs by the melanin-targeting ligands which brought one positive charge per grafted ligand when the tertiary amine is protonated.

Validation of the melanin-targeting ligand grafting to SRPs

Longitudinal proton relaxivity measurements. Since Gd(III) increases the spin lattice relaxation rate of water protons, chelates of the paramagnetic metal ion are commonly used as magnetic resonance contrast agents.[51] Relaxivity is an indicator of the efficiency with which the complex enhances the proton relaxation rates of water.[52] Longitudinal proton relaxivities of different SRPs at 60 MHz were calculated according to the following equation (eqn (1)):[51]

$$(1/T_1)_{\text{measured}} = (1/T_1)_{\text{water}} + r_1[\text{Gd}]_{\text{tot}} \quad (1)$$

where $T_{1\text{measured}}$ is the longitudinal relaxation time of the sample (ms), $T_{1\text{water}}$ is the longitudinal relaxation time of water (ms), r_1 is the longitudinal proton relaxivity of the sample (mM^{-1} s^{-1}) and $[Gd]_{tot}$ is the actual gadolinium concentration of the sample (mM) measured by ICP analysis. The slope of this line provides the molar relaxivity. Relaxivity values of water protons in the presence of SRPs are reported in Table 1.

Covalent conjugation of large molecular weight objects to imaging agents is likely to increase rotational correlation time, thus enhancing their relaxivity.[53,54] Indeed, at 60 MHz, the longitudinal relaxivities of the commonly utilized contrast agents such as Gd-DOTA (*e.g.* Dotarem®) and Gd-DTPA (*e.g.* Magnevist®) complexes are about 4 mM^{-1} s^{-1} while the longitudinal relaxivities of unfunctionalized SRPs equals 11.2 mM^{-1} s^{-1} and exceed 13 mM^{-1} s^{-1} for functionalized SRPs with melanin-targeting ligands. The small increase of the longitudinal relaxivities is in good agreement with an efficient functionalization of SRPs due to an increase of the correlation rotational time thanks to the augmentation of the particle's mass.

Mass Spectrometry (MS). The conjugation of melanin-targeting ligand **1** to SRPs was confirmed by mass spectrometry. First, SRPs were subjected to Electrospray Ionization (ESI) to generate intact ions in the gas phase and to obtain charge and mass information. The ESI spectrum of functionalized SRPs with melanin-targeting ligand **1** is reported in the ESI.† A multiplicative correlation algorithm (MCA) was used to estimate the mass of the SRPs from the mass-to-charge spectrum. The main distribution of SRP-**1** was divided into two parts: 8.7 kDa ± 0.4 kDa and 9.9 kDa ± 0.3 kDa.

At low mass in the negative mode, some details about the structure of the unfunctionalized SRPs had already been reported in earlier ESI-MS studies.[11] For example, it was noticed that the *m*/*z* 749 peak was specific to the $[Gd–DOTA–Si(OH)_3]^-$ fragment, namely the Gd–DOTA complex borne by a silanetriol, belonging to the polysiloxane network (Fig. 1(A)). The negative charge was shared out by the four carboxylic acids from the DOTA molecule. As expected, this peak was observed for both unfunctionalized and functionalized SRPs. An additional peak at *m*/*z* 630 was observed for both SRPs, matching an amide bond cleavage between DOTA and APTES molecules by loss of the $[NH(CH_2)_3Si(OH)_3]^-$ fragment.[55] This cleavage came with a C=C double bond creation and, as the Gd coordination number varies between 8 and 9,[56] a water molecule addition in its coordination sphere (Fig. 1(A)).

Table 1 Longitudinal relaxivities r_1 (mM^{-1} s^{-1}) of unfunctionalized and functionalized SRPs with melanin-targeting ligands at 60 MHz calculated according to eqn (1) and considering $(1/T_1)_{water}$ was negligible with respect to $(1/T_1)_{measured}$

Longitudinal proton relaxivities (mM^{-1} s^{-1}) at 60 MHz	
Unfunctionalized SRPs	11.2
SRP-**1**	13.4
SRP-**2**	13.0
SRP-**3**	14.4

Published on 12 December 2012 on http://pubs.rsc.org | doi:10.1039/C2NR33457G
Downloaded by University of California - San Diego on 21 January 2013

Then, in the positive mode, the low part of the ESI spectrum was dominated by the *m*/*z* 852 peak. This peak was observed for both unfunctionalized SRPs and functionalized SRPs with melanin-targeting ligand **1**. This *m*/*z* 852 peak was attributed to the Gd–DOTA complex borne by two APTES molecules belonging to the polysiloxane network (Fig. 1(B)). Finally, another peak was observed at *m*/*z* 991 and was specific to functionalized SRPs with melanin-targeting ligand **1**. As evidenced by the isotopic distribution (Fig. 1(B)), this peak was attributed to the [ligand **1**–DOTA–Si(OH)$_3$]$^+$ fragment, *i.e.* melanin-targeting ligand **1** conjugated to the DOTA chelate borne by a silanetriol (belonging to the polysiloxane network). The tertiary amine of melanin-targeting ligand **1** was protonated and gave the positive charge to the whole fragment. This *m*/z 991 fragment proves the covalent conjugation of the melanin-targeting ligand **1** to SRPs. It is interesting to note the absence of the Gd(III) ion within the DOTA ligand. It confirms the conjugation of the NH_2-ended ligands *via* one of the carboxylic acid functions from "free" DOTA molecules.

Infrared spectroscopy. IR measurements of unfunctionalized and functionalized SRPs with melanin-targeting ligands were performed to observe the covalent conjugation of the ligands to SRPs. IR spectra of the functionalized SRPs with melanin-targeting ligands were subtracted to the IR spectrum of unfunctionalized SRPs. The resulting spectra were overlaid to the IR spectrum of the corresponding melanin-targeting ligand (*e.g.* for SRP-**1**: see ESI†).

The spectrum of melanin-targeting ligand **1** displayed several characteristic peaks and bands at the following wavenumbers: 1671 cm^{-1} (C═O stretching vibrations of primary amides), 1592 cm^{-1} (N–H bending vibrations of primary amides), 1510–1580 cm^{-1} (C═C stretching vibrations of quinoxaline), 1472 cm^{-1} (C–H scissoring vibrations of –CH_2–), 1385 cm^{-1} (C–H symmetric bending vibrations of –CH_3), 1180–1350 cm^{-1} (C–N stretching vibrations of quinoxaline), 1030–1230 cm^{-1} (C–N stretching vibrations of primary and tertiary amines) and 700–900 cm^{-1} (C–H bending vibrations of quinoxaline and N–H bending vibrations of primary amines). On the spectrum resulting from the subtraction of functionalized SRPs with melanin-targeting ligand **1** to unfunctionalized SRPs, the 1580–1720 cm^{-1} large band increase indicated the presence of primary amide functions. These amide groups originate from the amide of melanin-targeting ligand **1** and from the formation of an amide bond between the primary amine of the ligand and the carboxylic acid of free DOTA molecules. Moreover, the increase of the two large bands at 1500–1560 cm^{-1} and 1000–1360 cm^{-1} might result from the presence of the quinoxaline and the tertiary amine, both coming from the melanin-targeting ligand **1**. This three band gain confirmed the covalent conjugation of melanin-targeting ligand **1** to SRPs. Similarly, the covalent conjugation of melanin-targeting ligands **2** and **3** to SRPs was demonstrated (see ESI†).

Quantification of the melanin-targeting ligand number per SRP

The absorption spectra of each melanin-targeting ligand displayed strong absorption bands in the UV region (256 and 342 nm for compounds **1** and **2**, 272 and 373 nm for compound **3**), which were assigned to the spin-allowed π–π* transition of the quinoxaline rings.[57] UV-visible absorption spectra of SRP-**1**, **2** and **3** are reported in the ESI.† These UV-visible absorption spectra were compared to each other before and after purification in order to evaluate the grafting rate of the melanin-targeting ligands to SRPs (with the hypothesis that coupling only slightly disturbs the molar extinction coefficient of the ligand). The two absorption bands assigned to melanin-targeting ligands **1**, **2** and **3** were observed, as well as a peak at 295 nm, specific to SRPs.

The final ligand/Gd molar ratios were about 0.4 for SRP-**1** and **3** and slightly lower (0.35) for SRP-**2**. The ligand/SRP molar ratios depend on the number of gadolinium atoms per SRP which was evaluated by elemental analysis.

Elemental analyses were performed on unfunctionalized and functionalized SRPs (see ESI†). The molar ratios deduced from weight percentages are reported in the ESI.† Two major hypotheses were made to estimate the SRP chemical compositions:[11]

(i) each SRP displays 10 ± 1 DOTA molecules;

(ii) the APTES/TEOS molar ratio of the polysiloxane network (1 Si = 0.6 APTES + 0.4 TEOS) remains constant during synthesis and purification steps.

The number of melanin-targeting ligands per SRP deduced by elemental analysis was in relatively good agreement with the values provided by UV-visible Absorption. The average numbers of melanin-targeting ligands per SRP exceeded 2 and equalled 2.5 for SRP-**1** and 2.2 for SRP-**2** and **3**.

Binding assays by surface plasmon resonance

Melanin is a biopolymer which chemical structure is still under debate; more specifically, the organization of its basic subunits is not clear yet.[35] Surface plasmon resonance was evidenced as a good test to highlight the binding of functionalized SRPs with melanin-targeting ligands to melanin for the reasons described below. Since studies involving the use of natural melanin require the isolation of the pigment from its biological environment without altering the pigment, synthetic melanin is generally preferred as a standard to natural melanin.[58,59] However, synthetic melanin is insoluble in almost all organic solvents,[35] which curbs the binding assays of SRPs to melanin in solution. In addition, melanin is characterized by a broadband absorption spectrum that increases exponentially towards the UV region,[36–38] which prevents the SRP detection in a melanin-containing solution. Finally, the similar molecular weights of both melanin polymers and SRPs made their separation by centrifugation really difficult. The inherent difficulties of performing optical spectroscopy on such macromolecules and their poorly understood heterogeneous structure have limited physical and chemical experiments. Consequently, we identified surface plasmon resonance as an interesting binding assay to melanin for the screening of functionalized SRPs with melanin-targeting ligands.

Binding assays of functionalized SRPs with melanin-targeting ligands to melanin were performed on a BIAcore®

Published on 12 December 2012 on http://pubs.rsc.org | doi:10.1039/C2NR33457G
Downloaded by University of California - San Diego on 21 January 2013

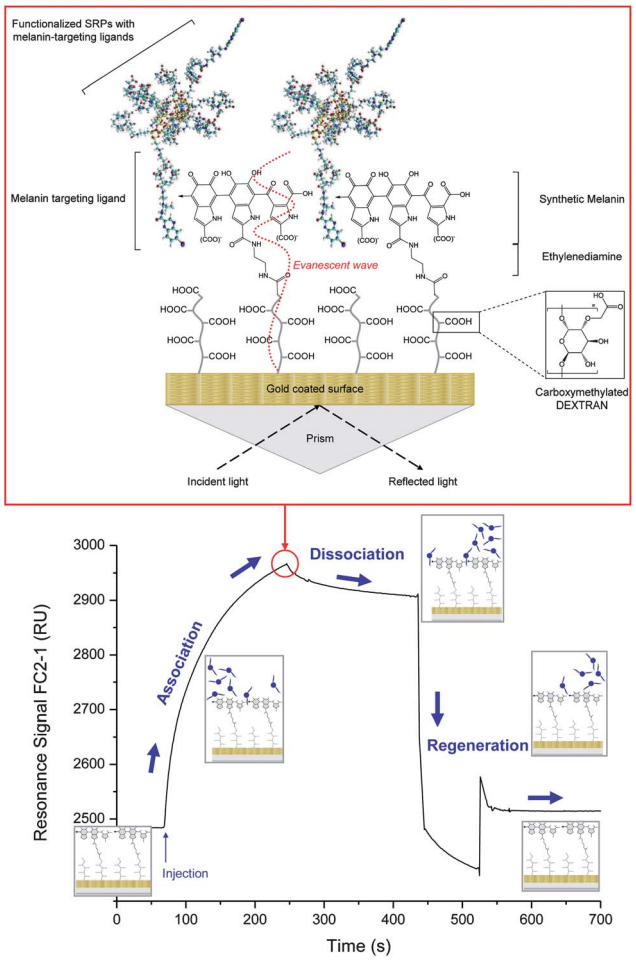

Fig. 2 Sensorgram of SRP-**1** ([Gd^{3+}] = 4.7 μM). The binding of functionalized SRPs with melanin targeting ligands to melanin 140 s after the end of the analyte injection (FC2) is represented in the red box above.

biosensor. Channel 2 was derivatized into a melanin surface to prove the binding of functionalized SRPs with melanin-targeting ligands to synthetic melanin (Fig 2 – red box). On the other hand, channel 1 was maintained in its carboxymethylated dextran native form in order to observe possible non-specific interactions.

Functionalized SRPs with melanin-targeting ligands as well as unfunctionalized SRPs were injected at different concentrations ([Gd^{3+}] ranging from 0.27 to 4.8 μM for functionalized SRPs with melanin-targeting ligands and from 5.6 to 714 μM for unfunctionalized SRPs). This range of concentrations allowed plotting the curve depicting the previously described relative response of the binding to melanin 140 s after the end of the analyte injection *versus* the Gd concentration of SRPs (Fig. 3(A) and (B)).

Then, the SRPs were injected at the same concentration ([Gd^{3+}] = 1 μM) to select the best applicant for melanin targeting (Fig. 4). The sensorgrams were collected as shown in Fig. 2. The resonance signal (FC2-FC1) obtained after subtraction of the signal generated by non-specific interactions with the dextran matrix (FC1) is displayed *versus* time. The *sensorgrams* of the four samples had the same profile. Moreover, the relative response on FC2-FC1, 140 s after the end of the analyte injection increased rapidly for low SRP concentrations; in contrast, this response tended to a much slower growth for higher SRP concentrations as if the binding sites began to saturate (Fig. 3(A) and (B)). In order to understand the influence of both ionic and hydrophobic sites on the binding to melanin, unfunctionalized and functionalized SRPs with melanin-targeting ligands were injected at the same concentration ([Gd^{3+}] = 1 μM) (Fig. 4).

An initial observation could be made: unfunctionalized SRPs seemed to have an affinity with melanin, most likely due to ionic interactions between the positive charges borne by the APTES molecules from SRPs and the negative charges of melanin. However, as expected, this affinity was much higher for functionalized SRPs with melanin-targeting ligands. Indeed, at the same concentration ([Gd^{3+}] = 1 μM), the FC2-FC1 signal is more than ten times higher for SRPs functionalized by melanin-targeting ligands (>58 RU) than for unfunctionalized SRPs (4.7 RU) (Fig. 4). This result confirmed that the melanin targeting is due to the ligands grafted on SRPs. A slight advantage might be attributed to SRP-**3**, then demonstrating the strong influence of the ionic interaction.

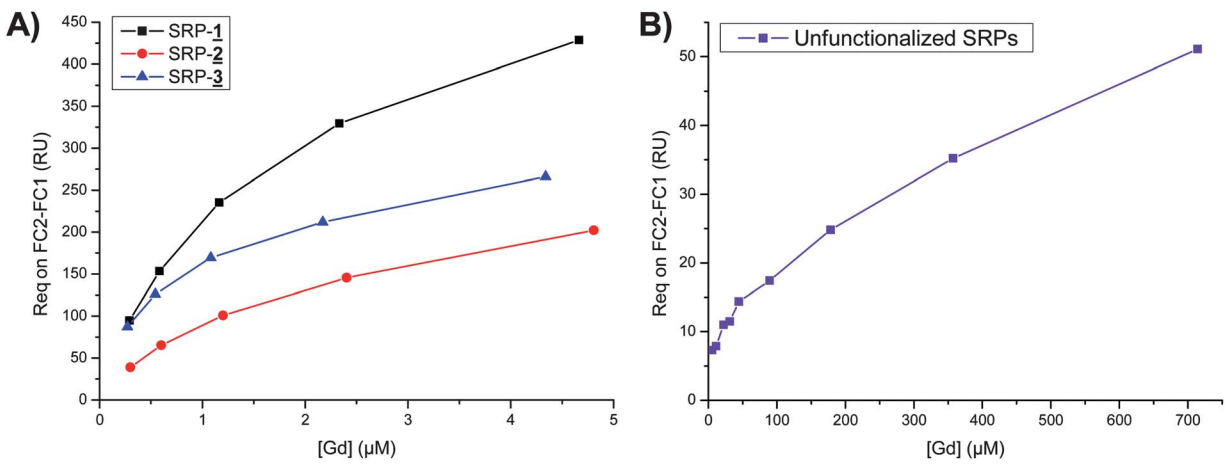

Fig. 3 BIAcore® analyses: relative response on the melanin surface (FC2-FC1) 140 s after the end of the analyte injection *versus* the concentration (in μM of Gd(III)) of (A) functionalized SRPs with melanin-targeting ligands **1**, **2** and **3** and (B) unfunctionalized SRPs.

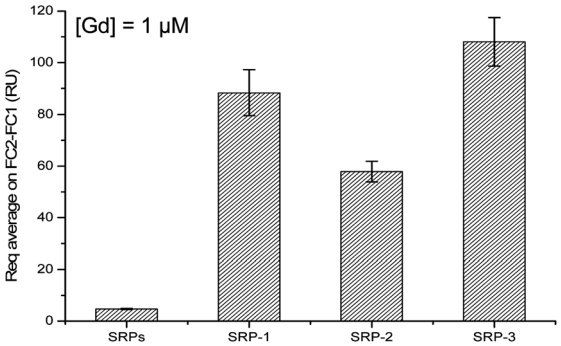

Fig. 4 BIAcore® analyses: relative response average and standard deviation on the melanin surface (FC2-FC1), 140 s after the end of the analyte injection at the same concentration ($[Gd^{3+}] = 1$ μM) for unfunctionalized SRPs and functionalized SRPs with melanin-targeting ligands **1**, **2** and **3**. The injection sequence (SRPs, SRP-**1**, SRP-**2**, SRP-**3**) was repeated 3 times.

Published on 12 December 2012 on http://pubs.rsc.org | doi:10.1039/C2NR33457G
Downloaded by University of California - San Diego on 21 January 2013

However, considering Fig. 3(A), the binding to melanin for SRP-**1** and **3** appeared to be quite similar for low concentrations ($[Gd^{3+}] < 1$ μM). Therefore, for low concentrations, neither of the two ligands (**1** and **3**) seems to prevail. In contrast, for higher concentrations, SRP-**1** emerged as the best candidate for melanin targeting. Indeed, melanin-targeting ligands **2** and **3** are equipped with a pegylated spacer arm whereas melanin-targeting ligand **1** is not. This spacer was added to take the ligand away from the SRP in order to ease melanin targeting. Surprisingly, this pegylated spacer appeared to hinder the binding of the ligand to melanin. As previously hypothesized, melanin-targeting ligands **2** and **3** might have bent on themselves, precisely thanks to their pegylated spacer. Since the melanin-targeting ligands bear a positive charge, they might have been attracted to the negative charges borne by the carboxylic acids of the DOTA ligands. This ionic interaction is likely to cause the bending of melanin-targeting ligands **2** and **3** on themselves and consequently to hinder their binding to melanin. In contrast, melanin-targeting ligand **1**, which is not equipped with a pegylated spacer, was not able to bend on itself, and this might be the reason of the higher binding of SRP-**1** to melanin compared to SRP-**2** and **3**. Consequently, no conclusion on the predominance of one of the two binding sites of the ligands on their binding to melanin could be drawn. However, these results confirm the affinity of the three ligands for melanin. This affinity results from the contribution of two interactions. First, an ionic interaction between the protonated tertiary amine of the melanin-targeting ligand and the synthetic melanin was highlighted in previous studies. On the other hand, the π stacking interactions between the aromatic rings of the melanin-targeting ligand and the aromatic ones of the melanin subunits add a stabilizing effect on the binding to melanin.[58]

Conclusions

Since malignant melanoma is one of the most difficult tumour types to treat, there is an urgent need to improve diagnosis and therapy for patients with disseminated melanoma. In this context, three quinoxaline derivatives were successfully synthesized as melanin seeking agents. Each of these three targeting molecules was covalently conjugated to SRPs in order to target the nanoparticles to melanin and therefore to melanoma. The grafting was confirmed and the average number of melanin-targeting ligands per SRP could be estimated and exceeded 2. Melanin targeting was observed *in vitro* using BIAcore®, a conventional surface plasmon resonance biosensor. The functionalized SRPs with the three different melanin-targeting ligands demonstrated high affinity for synthetic melanin compared to unfunctionalized SRPs. The binding to melanin is certainly the result of a strong ionic interaction, strengthened by a weaker but stable hydrophobic interaction. The functionalized SRPs with melanin-targeting ligand **1** appeared to be the best candidate for melanin targeting compared to SRP-**2** and **3**, of which the melanin-targeting ligands are equipped with a pegylated spacer. This active targeting, combined with the tremendous potential of SRPs to be detected by four complementary imaging techniques (MRI, SPECT, CT, fluorescence imaging) and to exhibit sensitizing properties for radiotherapy, supports the concept of an earlier and more accurate diagnosis and of an effective targeted radiotherapy for further *in vivo* studies.

Acknowledgements

This work was supported by the Canceropole Lyon Auvergne Rhône-Alpes for the proof of concept project LANTHARAD.

Notes and references

1 L. Finn, S. N. Markovic and R. W. Joseph, Therapy for metastatic melanoma: the past, present, and future, *BMC Med.*, 2012, **10**, 23.
2 C. Garbe, T. K. Eigentler, U. Keilholz, A. Hauschild and J. M. Kirkwood, Systematic review of medical treatment in melanoma: current status and future prospects, *Oncologist*, 2011, **16**, 5–24.
3 M. K. Khan, N. Khan, A. Almasan and R. Macklis, Future of radiation therapy for malignant melanoma in an era of newer, more effective biological agents, *OncoTargets Ther.*, 2011, **4**, 137–148.
4 A. P. Algazi, C. W. Soon and A. I. Daud, Treatment of cutaneous melanoma: current approaches and future prospects, *Cancer Manage. Res.*, 2010, **2**, 197–211.
5 P. Lorigan, T. Eisen and A. Hauschild, Systemic therapy for metastatic malignant melanoma – from deeply disappointing to bright future?, *Exp. Dermatol.*, 2008, **17**, 383–394.
6 J. A. Sosman, K. B. Kim, L. Schuchter, R. Gonzalez, A. C. Pavlick, J. S. Weber, G. A. McArthur, T. E. Hutson, S. J. Moschos, K. T. Flaherty, P. Hersey, R. Kefford, D. Lawrence, I. Puzanov, K. D. Lewis, R. K. Amaravadi, B. Chielowski, H. J. Lawrence, Y. Shyr, F. Ye, J. Li, K. B. Nolop, R. J. Lee, A. K. Joe and A. Ribas, Survival in BRAF V600-mutant advanced melanoma treated with vemurafenib, *N. Engl. J. Med.*, 2012, **366**, 707–714.

 This journal is © The Royal Society of Chemistry 2013

Published on 12 December 2012 on http://pubs.rsc.org | doi:10.1039/C2NR33457G
Downloaded by University of California - San Diego on 21 January 2013

7 M. R. Middleton, J. J. Grob, N. Aaronson, G. Fierlbeck, W. Tilgen, S. Seiter, M. Gore, S. Aamdal, J. Cebon, A. Coates, B. Dreno, M. Henz, D. Schadendorf, A. Kapp, J. Weiss, U. Fraass, P. Statkevich, M. Muller and N. Thatcher, Randomized phase III study of temozolomide *versus* dacarbazine in the treatment of patients with advanced metastatic malignant melanoma, *J. Clin. Oncol.*, 2000, **18**, 158–166.

8 G. A. Mc Arthur, I. Puzanov, R. Amaravadi, A. Ribas, P. Chapman, K. B. Kim, J. A. Sosman, R. J. Lee, K. Nolop, K. T. Flaherty, J. Callahan and R. J. Hicks, Marked, homogeneous, and early [^{18}F]fluorodeoxyglucose-positron emission tomography responses to vemurafenib in *BRAF*-mutant advanced melanoma, *J. Clin. Oncol.*, 2012, **30**, 1628–1634.

9 J. M. Chezal, J. Papon, P. Labarre, C. Lartigue, M. J. Galmier, C. Decombat, O. Chavignon, J. Maublant, J. C. Teulade, J. C. Madelomont and N. Moins, Evaluation of radiolabeled (hetero)aromatic analogues of *N*-(2-diethylaminoethyl)-4-iodobenzamide for imaging and targeted radionuclide therapy of melanoma, *J. Med. Chem.*, 2008, **51**, 3133–3144.

10 E. Dadachova, J. D. Nosanchuk, L. Shi, A. D. Schweitzer, A. Frenkel, J. S. Nosanchuk and A. Casadevall, Dead cells in melanoma tumors provide abundant antigen for targeted delivery of ionizing radiation by a mAb to melanin, *Proc. Natl. Acad. Sci. U. S. A.*, 2004, **101**(no. 41), 14865–14870.

11 F. Lux, A. Mignot, P. Mowat, C. Louis, S. Dufort, C. Bernhard, F. Denat, F. Boschetti, C. Brunet, R. Antoine, P. Dugourd, S. Laurent, L. Vander Elst, R. Muller, L. Sancey, V. Josserand, J. L. Coll, V. Stupard, E. Barbier, C. Rémy, A. Broisat, C. Ghezzi, G. Le Duc, S. Roux, P. Perriat and O. Tillement, Ultrasmall rigid particles as multimodal probes for medical applications, *Angew. Chem., Int. Ed.*, 2011, **50**, 12299–12303.

12 G. Le Duc, I. Miladi, C. Alric, P. Mowat, E. Bräuer-Krisch, A. Bouchet, E. Khalil, C. Billotey, M. Janier, F. Lux, T. Epicier, P. Perriat, S. Roux and O. Tillement, Toward an image-guided microbeam radiation therapy using gadolinium based nanoparticles, *ACS Nano*, 2011, **5**(no. 12), 9566–9574.

13 J. L. Bridot, D. Dayde, C. Rivière, C. Mandon, C. Billotey, S. Lerondel, R. Sabattier, G. Cartron, A. Le Pape, G. Blondiaux, M. Janier, P. Perriat, S. Roux and O. Tillement, Hybrid gadolinium oxide nanoparticles combining imaging and therapy, *J. Mater. Chem.*, 2009, **19**, 2328–2335.

14 H. S. Choi, W. Liu, F. Liu, K. Nasr, P. Misra, M. G. Bawendi and J. V. Frangioni, Design considerations for tumour-targeted nanoparticles, *Nat. Nanotechnol.*, 2010, **5**, 42–47.

15 A. S. Narang and S. Varia, Role of tumor vascular architecture in drug delivery, *Adv. Drug Delivery Rev.*, 2011, **63**(no. 8), 640–658.

16 H. S. Choi and J. V. Frangioni, Nanoparticles for biomedical imaging: fundamentals of clinical translation, *Mol. Imaging*, 2010, **9**(6), 291–310.

17 M. Benezra, O. Penate-Medina, P. B. Zanzonico, D. Schaer, H. Ow, A. Burns, E. DeStanchina, V. Longo, E. Herz, S. Iyer, J. Wolchok, S. M. Larson, U. Wiesner and M. S. Bradbury, Multimodal silica nanoparticles are effective cancer-targeted probes in a model of human melanoma, *J. Clin. Invest.*, 2011, **121**(no. 7), 2768–2780.

18 K. Jimbow, Y. Miyake, K. Homma, K. Yasuda, Y. Izumi, A. Tsutsumi and S. Ito, Characterization of melanogenesis and morphogenesis of melanosomes by physicochemical properties of melanin and melanosomes in malignant melanoma, *Cancer Res.*, 1984, **44**, 1128–1134.

19 J. M. Wood, K. Jimbow, R. E. Boissy, A. Slominski, P. M. Plonka, J. Slawinski, J. Wortsman and J. Tosk, What's the use of generating melanin?, *Exp. Dermatol.*, 1999, **8**, 153–164.

20 K. Sono, D. Lye, C. A. Moore, W. C. Boyd, T. A. Gorlin and J. M. Belitsky, Melanin-based coatings as lead-binding agents, *Bioinorg. Chem. Appl.*, 2012, article ID 361803.

21 K. Wakamatsu and S. Ito, Advanced chemical methods in melanin determination, *Pigm. Cell Res.*, 2002, **15**, 174–183.

22 S. E. McClain, K. B. Mayo, A. L. Shada, M. E. Smolkin, J. W. Patterson and C. L. Slingluff Jr, Amelanotic melanomas presebting as red skin lesions: a diagnostic challenge with potentially lethal consequences, *Int. J. Dermatol.*, 2012, **51**, 420–426.

23 A. Premkumar, F. Marincola, J. Taubenberger, C. Chow, D. Venzon and D. Schwartzentruber, Metastatic melanoma: correlation of MRI characteristics and histopathology, *Chin. J. Magn. Reson. Imaging*, 1996, **6**, 190–194.

24 A. Dadachova, J. D. Nosanchuk, L. Shi, A. D. Schweitzer, A. Frenkel, J. S. Nosanchuk and A. Casadevall, Dead cells in melanoma tumors provide abundant antigen for targeted delivery of ionizing radiation by a mAb to melanin, *Proc. Natl. Acad. Sci. U. S. A.*, 2004, **101**, 14865–14870.

25 E. Revskaya, A. M. Jongco, R. S. Sellers, R. C. Howell, W. Koba, A. J. Guimaraes, J. D. Nosanchuk, A. Casadevall and E. Dadachova, Radioimmunotherapy of experimental human metastatic melanoma with melanin-binding antibodies and in combination with dacarbazine, *Clin. Cancer Res.*, 2009, **15**, 2373–2379.

26 T. Q. Pham, I. Greguric, X. Liu, P. Berghofer, P. Ballantyne, J. Chapman, F. Mattner, B. Dikic, T. Jackson, C. Loc'h and A. Katsifis, Synthesis and evaluation of novel radioiodinated benzamides for malignant melanoma, *J. Med. Chem.*, 2007, **50**, 3561–3572.

27 I. Al Jammaz, B. Al-Otaibi, S. Okarvi and J. Amartey, Rapid and efficient synthesis of [^{18}F]fluoronicotamides, [^{18}F] fluoroisonicotamides and [^{18}F]fluorobenzamides as potential pet radiopharmaceuticals for melanoma imaging, *J. Labelled Compd. Radiopharm.*, 2011, **54**, 312–317.

28 C. Moura, T. Esteves, L. Gano, P. D. Raposinho, A. Paulo and I. Santos, Synthesis, characterization and biological evaluation of tricarbonyl M(I) (M = Re, ^{99m}Tc) complexes functionalized with melanin-binding pharmacophores, *New J. Chem.*, 2010, **34**, 2564–2578.

29 N. Moins, M. D'Incan, J. Bonafous, F. Bacin, P. Labarre, M. F. Moreau, D. Mestas, E. Noirault, F. Chossat, E. Berthommier, J. Papon, M. Bayle, P. Souteyrand, J. C. Madelmont and A. Veyre, ^{123}I-*N*-(2-diethylaminoethyl)-

Published on 12 December 2012 on http://pubs.rsc.org | doi:10.1039/C2NR33457G
Downloaded by University of California - San Diego on 21 January 2013

2-iodobenzamide: a potential imaging agent for cutaneous melanoma staging, *Eur. J. Nucl. Med.*, 2002, **29**, 1478–1484.

30 M. Eisenhut, W. E. Hull, A. Mohammed, W. Mier, D. Lay, W. Just, K. Gorgas, W. D. Lehmann and U. Haberkorn, Redioiodinated *N*-(2-diethylaminoethyl)benzamide derivatives with high melanoma uptake: structure-affinity relationships, metabolic fate, and intracellular localization, *J. Med. Chem.*, 2000, **43**, 3913–3922.

31 N. Desbois, M. Gardette, J. Papon, P. Labarre, A. Maisonial, P. Auzeloux, C. Lartigue, B. Bouchon, E. Debiton, Y. Blache, O. Chavignon, J. C. Teulade, J. Maublant, J. C. Madelmont, N. Moins and J. M. Chezal, Design, synthesis and preliminary biological evaluation of acridine compounds as potential agents for a combined targeted chemo-radionuclide therapy approach to melanoma, *Bioorg. Med. Chem.*, 2008, **16**, 7671–7690.

32 R. M. Ings, The melanin binding of drugs and its implications, *Drug Metab. Rev.*, 1984, **15**, 1183–1212.

33 M. Bonnet-Duquennoy, J. Papon, F. Mishellany, P. Labarre, J. L. Guerquin-Kern, T. D. Wu, M. Gardette, J. Maublant, F. Penault-Llorca, E. Miot-Noirault, A. Cayre, J. C. Madelmont, J. M. Chezal and N. Moins, Targeted radionuclide therapy of melanoma: anti-tumoural efficacy studies of a new ^{131}I labelled potential agent, *Int. J. Cancer*, 2009, **125**, 708–716.

34 J. C. Madelmont, J. M. Chezal, O. Chavignon, J. C. Teulade, N. Moins, Labelled analogues of halobenzamides as radiopharmaceuticals, World patent, WO2008012782, 2008.

35 K. Shanmuganathan, J. H. Cho, P. Iyer, S. Baranowitz and C. J. Ellison, Thermooxidative stabilization of polymers using natural and synthetic melanins, *Macromolecules*, 2011, **44**, 9499–9507.

36 F. Bernsmann, V. Ball, F. Addiego, A. Ponche, M. Michel, J. J. de Almeida Gracio, V. Toniazzo and D. Ruch, Dopamine–melanin film deposition depends on the used oxidant and buffer solution, *Langmuir*, 2011, **27**, 2819–2825.

37 P. Merdith, B. J. Powell, J. Riesz, S. P. Nighswander-Rempel, M. R. Pederson and E. G. Moore, *Soft Matter*, 2006, **2**, 37–44.

38 P. Meredith and J. Riesz, Radiative relaxation quantum yields for synthetic eumelanin, *Photochem. Photobiol.*, 2004, **79**(2), 211–216.

39 B. Liedberg, C. Nylander and I. Lundström, Biosensing with surface plasmon resonance – how it all started, *Biosens. Bioelectron.*, 1995, **10**, i–ix.

40 S. Lin, A. S. Y. Lee, C. C. Lin and C. K. Lee, Determination of binding constant and stoichiometry for antibody-antigen interaction with surface plasmon resonance, *Curr. Proteomics*, 2006, **3**, 271–282.

41 D. A. Edwards, Steric hindrance effects on surface reactions: applications to BIAcore, *J. Math. Biol.*, 2007, **55**, 517–539.

42 Y. Taguchi, E. Takano and T. Takeuchi, SPR sensing of bisphenol a using molecularly imprinted nanoparticles immobilized on a slab optical waveguide with consecutive parallel Au and Ag deposition bands coexistent with bisphenol 1 – immobilized Au nanoparticles, *Langmuir*, 2012, **28**, 7083–7088.

43 T. Ghosh, L. Williams and C. H. Mastrangelo, Label-free detection of protein binding with multisine SPR microchips, *Lab Chip*, 2011, **11**, 4194–4199.

44 W. L. F. Armarego and D. D. Perrin, *Purification of Laboratory Chemicals*, ed. Butterworth and Heinemann, Reed educational and professional Publishing Ltd, Oxford, 4th edn, 1996.

45 B. Johnsson, S. Löfås and G. Lindquist, Immobilization of proteins to a carboxymethyldextran-modified gold surface for biospecific interaction analysis in surface plasmon resonance sensors, *Anal. Biochem.*, 1991, **198**, 268–277.

46 K. Q. Ling and L. M. Sayre, Discovery of a sensitive, and tightly binding fluorogenic substrate of bovine plasma amine oxidase, *J. Org. Chem.*, 2009, **74**, 339–350.

47 J. H. Jones, W. J. Holtz and E. J. Cragoe, 6-Substituted 5-chloro-1,3-dihydro-2*H*-imidazo[4,5-*b*]pyrazin-2-ones with hypotensive activity, *J. Med. Chem.*, 1973, **16**, 537–542.

48 D. Denoyer, P. Labarre, J. Papon, E. Miot-Noirault, M. J. Galmier, J. C. Madelmont, J. M. Chezal and N. Moins, Development of high-performance liquid chromatographic method for the determination of a new potent radioiodinated melanoma imaging and therapeutic agent, *J. Chromatogr., B: Anal. Technol. Biomed. Life Sci.*, 2008, **875**, 411–418.

49 M. Alterman, H. Sjöbom, P. Säfsten, P. O. Markgren, U. H. Danielson, M. Hämäläinen, S. Läfas, J. Hultén, B. Classon, B. Samuelsson and A. Hallberg, P1/P1′ modified HIV protease inhibitors as tools in two new surface plasmon resonance biosensor screening assays, *Eur. J. Pharm. Sci.*, 2001, **13**, 203–212.

50 L. You, S. Feng, R. An, X. Wang and D. Bai, Silica gel accelerated aza-Michaël addition of amines to α,β-unsaturated amides, *Tetrahedron Lett.*, 2008, **49**, 5147–5149.

51 N. Fatin-Rouge, E. Tóth, R. Meuli and J. C. G. Bünzli, Enhanced imaging properties of a Gd^{III} complex with unusually large relaxivity, *J. Alloys Compd.*, 2004, **374**, 298–302.

52 R. B. Lauffer, Paramagnetic metal complexes as water proton relaxation agents for NMR imaging: theory and design, *Chem. Rev.*, 1987, **87**, 901–927.

53 A. Ghosh, M. Haverick, K. Stump, X. Yang, M. F. Tweedle and J. E. Goldberger, Fine-tuning the pH trigger of self-assembly, *J. Am. Chem. Soc.*, 2012, **134**, 3647–3650.

54 S. R. Bull, M. O. Guler, R. E. Bras, T. J. Meade and S. I. Stupp, Self-assembled peptide amphiphile nanofibers conjugated to MRI contrast agents, *Nano Lett.*, 2004, **5**, 1.

55 A. G. Harrison, K. W. M. Siu and H. El Aribi, Amide bond cleavage in deprotonated tripeptides: a newly discovered pathway to 'b2 ions', *Rapid Commun. Mass Spectrom.*, 2003, **17**, 869–875.

56 C. A. Chang, L. C. Francesconi, M. F. Malley, K. Kumar, J. Z. Gougoutas and M. F. Tweedle, Synthesis, characterization and crystal structures of M(DO3A) (M = Fe, Gd) and Na[M(DOTA)] (M = Fe, Y, Gd), *Inorg. Chem.*, 1993, **32**, 3501–3508.

57 F. M. Hwang, H. Y. Chen, P. S. Chen, C. S. Liu, Y. Chi, C. F. Shu, F. I. Wu, P. T. Chou, S. M. Peng and G. H. Lee,

 This journal is © The Royal Society of Chemistry 2013

Iridium(III) complexes with orthometalated quinoxaline ligands: subtle tuning of emission to the saturated red color, *Inorg. Chem.*, 2005, **44**, 1344–1353.

58 M. Borel, D. Lafarge, M. F. Moreau, M. Bayle, L. Audin, N. Moins and J. C. Madelmont, High resolution magic angle spinning NMR spectroscopy used to investigate the ability of drugs to bind to synthetic melanin, *Pigm. Cell Res.*, 2005, **18**, 49–54.

59 L. Gautam, K. S. Scott and M. D. Cole, Amphetamine binding to synthetic melanin and scatchard analysis of binding data, *J. Anal. Toxicol.*, 2005, **29**, 339–344.

Downloaded by University of California - San Diego on 21 January 2013
Published on 12 December 2012 on http://pubs.rsc.org | doi:10.1039/C2NR33457G